13 May 2024

ALMA MATER STUDIORUM
UNIVERSITÀ DI BOLOGNA

ARCHIVIO ISTITUZIONALE
DELLA RICERCA

Alma Mater Studiorum Università di Bologna
Archivio istituzionale della ricerca

Increased efficiency and stability of Dye-Sensitized Solar Cells (DSSC) photoanode by intercalation of Eosin Y into Zn/Al layered double hydroxide

This is the final peer-reviewed author's accepted manuscript (postprint) of the following publication:

Published Version:
Increased efficiency and stability of Dye-Sensitized Solar Cells (DSSC) photoanode by intercalation of Eosin Y into Zn/Al layered double hydroxide / Fasolini, Andrea; Sangiorgi, Nicola; Tosi Brandi, Eleonora; Sangiorgi, Alex; Mariani, Federica; Scavetta, Erika; Sanson, Alessandra; Basile, Francesco. - In: APPLIED CLAY SCIENCE. - ISSN 0169-1317. - STAMPA. - 212:(2021), pp. 106219.1-106219.10. [10.1016/j.clay.2021.106219]

This version is available at: https://hdl.handle.net/11585/862568 since: 2023-05-09

Published:

DOI: http://doi.org/10.1016/j.clay.2021.106219

Terms of use:

Some rights reserved. The terms and conditions for the reuse of this version of the manuscript are specified in the publishing policy. For all terms of use and more information see the publisher's website.

(Article begins on next page)

This item was downloaded from IRIS Università di Bologna (https://cris.unibo.it/).
When citing, please refer to the published version.

This is the final peer-reviewed accepted manuscript of:

Andrea Fasolini, Nicola Sangiorgi, Eleonora Tosi Brandi, Alex Sangiorgi, Federica Mariani, Erika Scavetta, Alessandra Sanson, Francesco Basile, Increased efficiency and stability of Dye-Sensitized Solar Cells (DSSC) photoanode by intercalation of Eosin Y into Zn/Al layered double hydroxide, Applied Clay Science, Volume 212, 2021, 106219,

The final published version is available online at: **https://doi.org/10.1016/j.clay.2021.106219**

Terms of use:

Some rights reserved. The terms and conditions for the reuse of this version of the manuscript are specified in the publishing policy. For all terms of use and more information see the publisher's website.

Increased efficiency and stability of Dye-Sensitized Solar Cells (DSSC) photoanode by intercalation of Eosin Y into Zn/Al layered double hydroxide

Andrea Fasolini [a]*, Nicola Sangiorgi [b], Eleonora Tosi Brandi [a], Alex Sangiorgi [b], Federica Mariani [a], Erika Scavetta [a], Alessandra Sanson [b], Francesco Basile [a]*.

[a] Department of Industrial Chemistry "Toso Montanari", Alma Mater Studiorum—University of Bologna, Viale del Risorgimento 4, 40136 Bologna, Italy

[b] Institute of Science and Technology for Ceramics – National Research Council of Italy (ISTEC-CNR), Via Granarolo 64, 48018 Faenza (RA), Italy

*Correspondi Authors: Francesco Basile (f.basile@unibo.it), Andrea Fasolini (andrea.fasolini2@unibo.it)

Abstract

Layered Double Hydroxides (LDH) are versatile materials that can be applied to different fields. Recently their employment in Dye-Sensitized Solar Cells (DSSCs) technology has been reported. The heart of this technology is the photoanode, a semiconductor layer sensitized with dye molecules able to absorb the sunlight. However, the traditional dye molecules are quite expensive and sensitive to thermal degradation and the sensitization process requires time and costs. The possibility to directly intercalate the dye in the LDH interlayer makes these materials very promising as innovative photoanodes. This aspect in fact would help to reduce both the time and the costs, overcome charge-transfer and recombination phenomena issues and finally increase the Photo-Conversion Efficiency (PCE) and stability. In this work, an Eosin Y-intercalated ZnAl LDH was prepared by coprecipitation and applied as photoanode material. For this purpose, a screen-printing ink was formulated and then applied onto a conductive transparent substrate. Then, complete DSSC prototypes were assembled and tested. A comparison with an analogous LDH intercalated with terephthalate and sensitized with Eosin Y showed a beneficial effect due to the presence of the dye intercalated in the structure rather than adsorbed on the surface, increasing the stability (tested for 1500 hours) and efficiency of the related DSSCs. A 0.11 mA cm^{-2} of J_{SC}, 568 mV of V_{OC} and a PCE of 0.019% were obtained for the Eosin Y intercalated LDH based photoanode. Moreover, the interaction between the intercalated dye and the LDH sheets allowed to reduce charge recombination phenomena and thus to increase V_{OC} and PCE values.

Keywords: Zn/Al Layered Double Hydroxides, Coprecipitation method, Dye-Sensitized Solar Cells (DSSC), dye intercalation, photoanode, light absorption, charge recombination.

Introduction

Layered double hydroxides (LDH) are anionic clays, with the general formula $M(II)_{1-x}M(III)_x(OH)_2]^{x+}(A^{n-}_{x/n}).mH_2O$, largely employed in different fields (Cavani et al., 1991a; Xu et al., 2011; Z. Yang et al., 2016; Mishra et al., 2018), from sensors (Baig and Sajid, 2017; Asif et al., 2018; Tang et al., 2020), polymer additives (Jin et al., 2020), drug delivery (Barkhordari and Yadollahi, 2016; Shahabadi and Razlansari, 2018), cosmetics (Li et al., 2017) and absorbers (F. Yang et al., 2016; Abdellaoui et al., 2017; Zubair et al., 2017; Daud et al., 2019) to catalysts and catalyst precursors (Cavani et al., 1991a; Basile et al., 2002, 2004; F Basile et al., 2010; F. Basile et al., 2010; Xu et al., 2011; Monti et al., 2013; Fasolini et al., 2019; Gjyli et al., 2019; Tabanelli et al., 2019), electrocatalysis (Wang et al., 2018), photocatalysis (Mohapatra and Parida, 2016; J. Wu et al., 2018; Rasouli, 2018; Darie et al., 2019; Zhang et al., 2020) and photo-electrochemistry (Arif et al., 2020; Luo et al., 2020; Zhang et al., 2021). An interesting application in which LDH could play an important role and which has not been widely explored yet is as photoanode material for Dye-Sensitized Solar Cells (DSSCs). These solar cells are usually composed of a semiconductor sensitized with a dye molecule, a counter electrode and a liquid electrolyte to close the circuit (Benesperi et al., 2018). Up to now, LDH have been used in DSSCs mainly as gelling agents for liquid electrolytes to increase the device stability (Bastianini et al., 2014; Du et al., 2015). Traditionally, DSSCs photoanode is composed by TiO_2, sensitized with organic or metallorganic dyes (Bendoni et al., 2016), or, by perovskites (Park, 2015). Recently, due to the high surface area and easily synthetic procedure, different LDH based on NiAl (Foruzin et al., 2019), ZnTi (Liu et al., 2019), ZnAl (Tadanaga et al., 2016; Zhu et al., 2017) and composites with ZnO (Salih et al., 2019) and TiO_2 (Foruzin et al., 2019) were prepared, sensitized with commercial or organic dyes (L. Pinto et al., 2019) and finally tested as DSSC photoanode. Nevertheless, the layered and versatile LDH structure could be used to directly incorporate the dye molecules. This approach helps to overcome the traditional issues related to charge-transfer and recombination phenomena that typically occur at the interfaces TiO_2/dye/electrolyte that reduce the final Photo-Conversion Efficiency (PCE). Moreover, the long-term stability of the related DSSCs should be improved by incorporating the dye directly in the crystal structure of the photoanode material, thus avoiding the corrosive action of the electrolyte. Finally, the production process of traditional DSSCs would be reduced in terms of time and costs by removing the sensitization step. Literature reports just one work that proposes the intercalation of the active dye inside the interlayers of a ZnAl LDH through a hot water sol-gel process for the application in DSSCs. However, no value of DSSCs efficiency or detailed characterizations were discussed (Tadanaga et al., 2016). Thus, this study aims to provide a deeper understanding of the performances of dye intercalated LDH applied as DSSC photoanodes. Usually, LDH are synthesized using carbonate anions due to the ease of synthesis and the possibility of facile carbonate decomposition by calcination

to directly obtain mixed oxides (Cavani et al., 1991b). Nevertheless, any anion can be theoretically intercalated into LDH and a variety of them has been reported (Rives and Angeles Ulibarri, 1999; Costantino et al., 2008; Conterosito et al., 2018), from the more classical NO_3^- and halogens (Meng et al., 2004), or silicates (Albertazzi et al., 2007; Basile et al., 2009) to organic molecules such as terephthalate (Vucelic et al., 1995), dyes (Zaghouane-Boudiaf et al., 2012; Gao et al., 2017; Gao and Yan, 2017a; Gao et al., 2018; Daud et al., 2019; Prasad et al., 2019) or porphyrins (Wypych et al., 2003; Káfuňková et al., 2010) until to cellulose (Kang et al., 2009; Yadollahi et al., 2014; Iftekhar et al., 2017), graphene (Cao et al., 2016; Daud et al., 2016), drugs (Ladewig et al., 2009) or DNA (Desigaux et al., 2006; Oh et al., 2006). Different methodologies have been investigated to produce LDH with the desired anion in the interlayer (Conterosito et al., 2013, 2018). For example, acid-base exchange or diffusion-controlled reactions (Iyi et al., 2011; Conterosito et al., 2013) can lead to the substitution of an anion with an inorganic or organic one. Anions can also be inserted by a reconstruction mechanism, in which an LDH is transformed into a mixed oxide and then immersed in a solution containing the desired anion that contributes to the reformation of a differently intercalated LDH (Guo et al., 2013). The intercalated anion can also be substituted by liquid-assisted grinding in which an LDH is ground in the presence of a small amount of solvent where the target anion is dissolved (Milanesio et al., 2010). However, these methods require a multi-step synthesis, where the desired anion is inserted in a second moment. In this work, we selected the classical coprecipitation of cations into an aqueous solution where the anion is dissolved, as a one-pot, facile, reliable, fast and energy-efficient method to produce LDH for DSSC applications. In particular, a ZnAl-based LDH was selected because this composition is the one suitable for DSSCs application (Tadanaga et al., 2016; Liu et al., 2019; Zhu et al., 2017) and because zinc is one of the most used metal for photoanodes productions (ZnO form). Eosin Y dye (Figure 1) was selected as intercalated anion due to its high absorption coefficient, low-cost and ease of handling, and finally for its metal-free structure. This method is simpler and more easily scalable than one-pot synthesis involving microwave, hydrothermal or sonication, which were thus not considered. The intercalation of Eosin Y in the LDH structure (**LDH-E)** allows to obtain a peculiar interaction between the dye and the inorganic framework, which may favour electron transfer, if compared to the classical surface adsorption of the dye. To prove this, the synthesized LDH was compared with a ZnAl LDH intercalated with a non-dye anion (terephthalate; **LDH-T** Figure 1). Although classical synthesis of LDH incorporates CO_3^{2-} anions in the interlayer, terephthalate anion was chosen in this work for comparison with Eosin, to obtain LDH with similar interlayer height, which may affect the electrostatic and H bond interaction, as well as the photoelectrochemical properties of the materials. The as-obtained powders were characterized by XRD, TEM and TGA and were used to prepare the

screen-printing inks and the correspondent films. These films were used as photoanodes for DSSCs application and deeply characterized from the photovoltaic and electrochemical points of view. Finally, the long-term stability of the obtained devices was evaluated. The PCE and electrochemical properties were found to be higher than the one found in the literature (Tadanaga et al., 2016) demonstrating for the first time the beneficial effects of the direct dye intercalation inside the LDH structure. In particular, a current density of 0.11 mA cm^{-2}, open circuit potential of 568 mV and a PCE of 0.019% were achieved in this work compared with 0.060 mA cm^{-2} and 300 mV reported in the literature (Tadanaga et al., 2016).

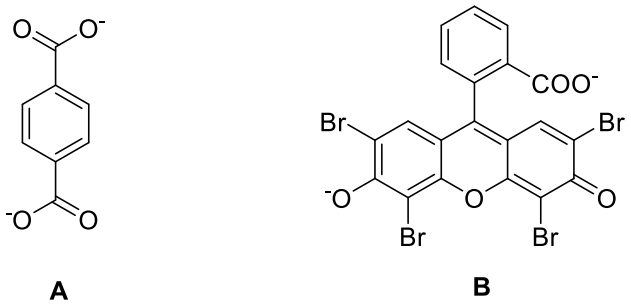

Figure 1. Chemical structure of (A) terephthalate and (B) Eosin anions.

2. Experimental

2.1 Synthetic procedure

The Eosin intercalated and the terephthalate intercalated layered double hydroxides, named **LDH-E** and **LDH-T**, respectively, were synthesized by coprecipitation at constant pH. Eosin Y (99%, Sigma Aldrich, 0.014 mol, 9.09 g,) or sodium terephthalate (99%, Sigma Aldrich, 0.014 mol, 2.97 g,) were dissolved in 140 ml of water kept at pH 9.5. The solution was heated to 60°C and kept under vigorous stirring. $Zn(NO_3)_2 \cdot 6H_2O$ (99%, Sigma Aldrich 0.014 mol, 4.17 g) and $Al(NO_3)_3 \cdot 9H_2O$ (99%, Sigma Aldrich, 0.007 mol, 2.69 g) were dissolved in 10.5 ml of distilled water and added dropwise to the solution containing Eosin Y or sodium terephthalate. The pH was kept at 9.5 by the addition of a 1.5 M NaOH aqueous solution. The resulting suspension was aged for 1 h at 60°C under stirring. The obtained solid was filtered, washed with distilled water up to neutral pH and dried at 70°C overnight. Distilled water was bubbled with nitrogen for 3 h before the synthesis to remove eventually dissolved carbonates. The solutions were kept under nitrogen atmosphere to avoid the dissolution of CO_2 from air.

2.2 Sample characterizations

X-ray diffraction (XRD) analyses were carried out with a Philips PW1050/81 diffractometer equipped with a graphite monochromator in the diffracted beam and controlled by a PW1710 unit (Cu Kα, λ =0.15418 nm). A 2θ range from 5° to 80° was investigated at a speed of 0,05°/s. Low angle analysis, between 2° and 16° (0,05°/s) with narrower slits, had to be carried out in a separate experiment, as the X-ray coming from the source would hit the detector without diffracting, increasing the noise of the analysis. TEM analyses were performed with a TEM/STEM FEI TECNAI F20 microscope combined with Energy Dispersive X-Ray Spectrometry (EDS), at 200 keV. The powder was first suspended in ethanol and treated with an ultrasonic probe for 15 min, then deposited on a "multifoil-carbon film" sustained by a Cu grid. Thermogravimetric analyses (TGA) were performed on a TA Instruments SDT Q600, under air atmosphere (flow rate: 100 ml/min) heating ramp of 5°C/min from 25 °C to 200 °C with a dwelling time of 30 minutes at this temperature and at 5°C/min up to 600°C followed by 120 minutes isotherm. Reflectance UV-VIS tests were performed on the as-prepared powders after drying at 70°C in a Perkin Elmer Lambda 19 in the range 180-800 nm.

2.3 Inks formulation and films deposition

Two different screen-printing inks were formulated containing the LDH-T or the LDH-E compound. Screen-printing inks were prepared by mixing the respective powders with organic additives: terpineol (Sigma-Aldrich) as solvent, lauric acid as dispersant (Merck, Germany), ethyl cellulose as binder (Sigma-Aldrich, Germany) and finally, glycerol (Merck, Germany) as plasticizer. The powders were firstly dispersed in the solvent and the different organics were added to obtain a stable suspension. The as-formulated inks were finally homogenized in a three-roll mill equipped with ZrO_2 rollers (Exakt 80E, Exakt, Nordestedt, Germany). LDH based inks were deposited onto TiO_2 blocking layer coated Fluorine-doped Tin Oxide (FTO) glass substrates (sheet resistance 7 Ω/sq, Sigma-Aldrich) using a semi-automatic screen-printer (AUR'EL 900, AUR'EL Automation s.p.a., Italy) (Sangiorgi et al., 2014). The films were dried by an IR thermal treatment performed at 180°C for 3 hours to avoid the LDH and Eosin Y degradation. To confirm it, XRD was carried out on the LDH-E powder after the drying at 180°C, which showed that the pattern of the LDH structure was still present and was coherent with the intercalation of Eosin in the interlayer (Figure S1) and showed the same interlayer distance (Figure S2). A lower crystallinity of the reflects related to the 009 Miller index and partially to the 006 were observed due to a partial loss of interlayer water, after the thermal treatment. The thickness of each film was set at 12 μm as confirmed by profilometry.

2.4 DSSCs assembly

LDH-T and LDH-E photoanodes were kept at 100°C for 30 minutes, in order to eliminate air moisture. The sensitization process on LDH-T was done immerging the photoanodes in 0.003 M

ethanol solutions of Eosin Y dye for 18 hours to assure the complete sensitizer uptake (sample named **LDH-T+Eosin**). A pre-drilled FTO glass, coated with a sputtered platinum thin layer, was used as counter-electrode. After sensitization, the electrodes were assembled into a sandwich-type cell and sealed with a hot-melt gasket made of Meltonix (thickness 25 µm, Solaronix, Switzerland). The electrolyte (Iodolyte Z100, Solaronix, Switzerland) was introduced in the cell via vacuum back-filling through the hole at the counter electrode. Finally, the hole was sealed using a Meltonix (Solaronix, Switzerland) film and a small cover glass. The active area of the solar cells was fixed at 0.25 cm^2.

2.5 DSSCs tests

To evaluate the DSSC cells' performance, J-V curves were collected under 1000 W m^{-2} AM 1.5 G illumination (calibrated with a reference standard silicon cell) using an Abet Technologies Solar Simulator (SUN 2000, USA) and a Keithley 2400 source/meter (Keithley, USA). The Incident Photon-to-Current Conversion Efficiency (IPCE) was quantified with an IPCE PVE300 system (Bentham, United Kingdom) with a dual Xenon/Quartz halogen light source, in the wavelength range between 300 and 750 nm. EIS analyses were recorded over a frequency range of 10^5 Hz to $5x10^{-2}$ Hz with an amplitude of 10 mV at the Voc in the dark. All the electrochemical characterizations were carried out with an AUTOLAB PGSTAT302N-FRA32M (Eco Chemie, the Netherlands) and elaborated using Nova 2.1 software. The EIS analyses were fitted by Z-View software (Scribner Associates). Finally, long-term stability tests were done on the obtained DSSCs. The devices were stored in the dark at room temperature and pressure for 1500 hours and the J-V curves were acquired during the whole period.

3. Results and discussion

3.1. Structure and morphology of the obtained samples

The coprecipitation synthesis was used to produce intercalated Eosin Y (LDH-E) and sodium terephthalate (LDH-T) as anions into the layered double hydroxide structure. Powder X-ray diffractograms of the obtained samples are shown in Figure 2A. Both samples show reflections that are commonly ascribed to the pattern of LDH (Cavani et al., 1991a). In particular, the samples show 6 main reflections centred at 4.6° (003), 10.4° (006), 14.6° (009), 24.1° (0012), 34.1° (0015) and 60.6° (110) for LDH-E and at 6.5° (003), 12.7° (006), 19.1° (009), 25.4° (0012), 34.1° (0015) and 60.6° (0015) for LDH-T. To better identify the low angle peaks of LDH-E, an analysis from 2° to 16° was carried out which is reported in Figure 2B. A good multiple relationship between d values of basal (003), second order (006) and third order (009) reflections is observed, which is characteristic of layered double hydroxide structure and indicative of the width of the interlayer containing the

anion (Gao and Yan, 2017b). This value is given by the lattice parameter *c*, which can be calculated from the d values of these reflections: $c = 1/3(d_{003} + 2d_{006} + 3d_{009})$. The obtained values are reported in Table 1. These values highlight a clear difference among the two samples, namely the d values and consequently the *c* parameter. In fact, the reflections are shifted toward lower angles for LDH-E. This results in a higher *c* parameter which entails a larger gap between the hydroxide sheets of the layered double hydroxide. As expected, Eosin Y, which is a bigger anion than terephthalate, contributes to increasing the width of the interlayer. Noteworthy, the lattice parameter *c* of the two samples is consistent with the dimension of the two interlayered molecules (Table 1), which further confirms the success of the synthesis. Another difference found between the diffractograms is the crystallinity degree, which is correlated to the full width at half maximum of the peaks (FWHM). Average crystallite dimension was calculated with the Scherrer equation for the reflects at low angles (4.7°, 10.4° and 14.6° for LDH-E and 6.3° 12.8° and 19.1° for LDH-T), which indicates the crystallite size in the stacking direction. It resulted to be 5.4 and 21.4 nm respectively. The low intensity of the reflection and the presence of shoulders did not allow the calculation at higher angles. LDH-T is highly crystalline while a lower crystallinity degree is displayed by LDH-E. Nevertheless, this synthetic method allowed to obtain more crystalline materials compared to the sol-gel method reported in the literature for the preparation of ZnAl-Eosin LDH systems (Tadanaga et al., 2016)

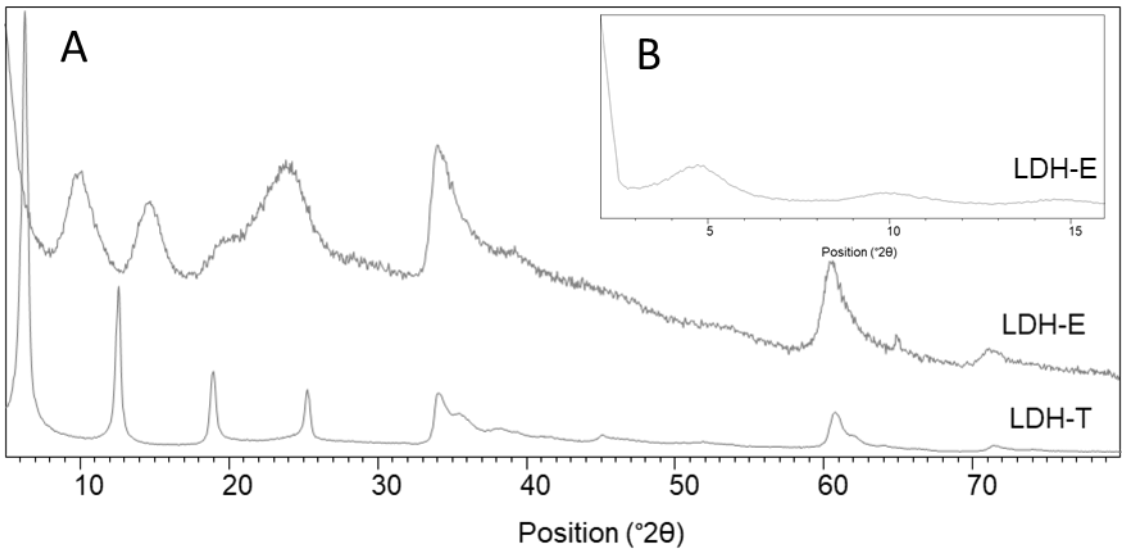

Figure 2. X-ray diffraction analysis of LDH-E (yellow) and LDH-T (red) obtained by coprecipitation: (A) XRD analysis of both samples from 5° to 80°2θ; (B) XRD analysis of LDH-E from 2° to 16°2θ.

Table 1. d values of basal (003) second order (006) and third order (009) reflections and lattice parameter c for LDH-E and LDH-T.

Sample	d_{003} (nm)	d_{006} (nm)	d_{009} (nm)	Anion dimension (nm)	*c* (nm)
LDH-E	1.91	0.84	0.60	1.03	1.80
LDH-T	1.38	0.69	0.46	0.70	1.38

TEM analysis was used to probe the morphology of the LDH-E sample at low scales. This showed the presence of channels and continuous stacked layers with a wide length. Interestingly, the distance between the observed layers is 1.85 nm, which is consistent with the lattice parameter *c* observed with XRD analysis and the intercalation of Eosin Y molecule.

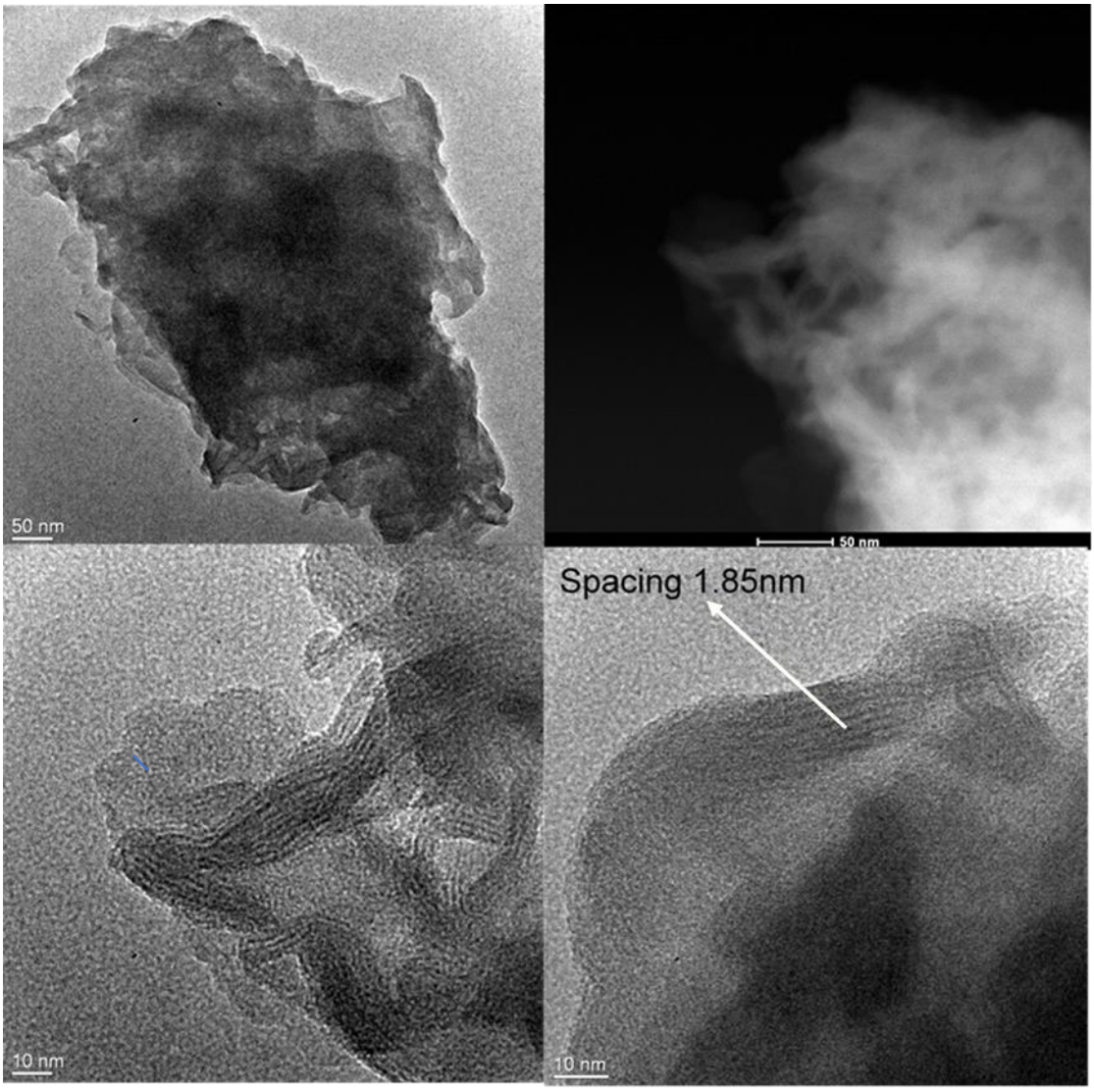

Figure 3. TEM images of LDH-E.

The thermal stability of LDH-E and LDH-T was evaluated by TGA/DTG (Figure 4). The analysis of the former shows four degradation steps. The first one, below 200°C, corresponds to the removal of water from the LDH interlayer (Ahmed et al., 2012). The three other peaks are related to the dehydration of the hydroxide layer and the decomposition of the Eosin Y anion and hydroxide

decomposition to mixed oxide (Cavani et al., 1991a; Ahmed et al., 2012). In general, the material is stable up to 200°C while a fast decomposition is observed at higher temperatures. LDH-T also shows a weight loss below 200°C due to water loss, together with a sharp reduction in weight around 450°C. The latter is due to the decomposition of terephthalate anion and of the LDH structure as typical for these materials.

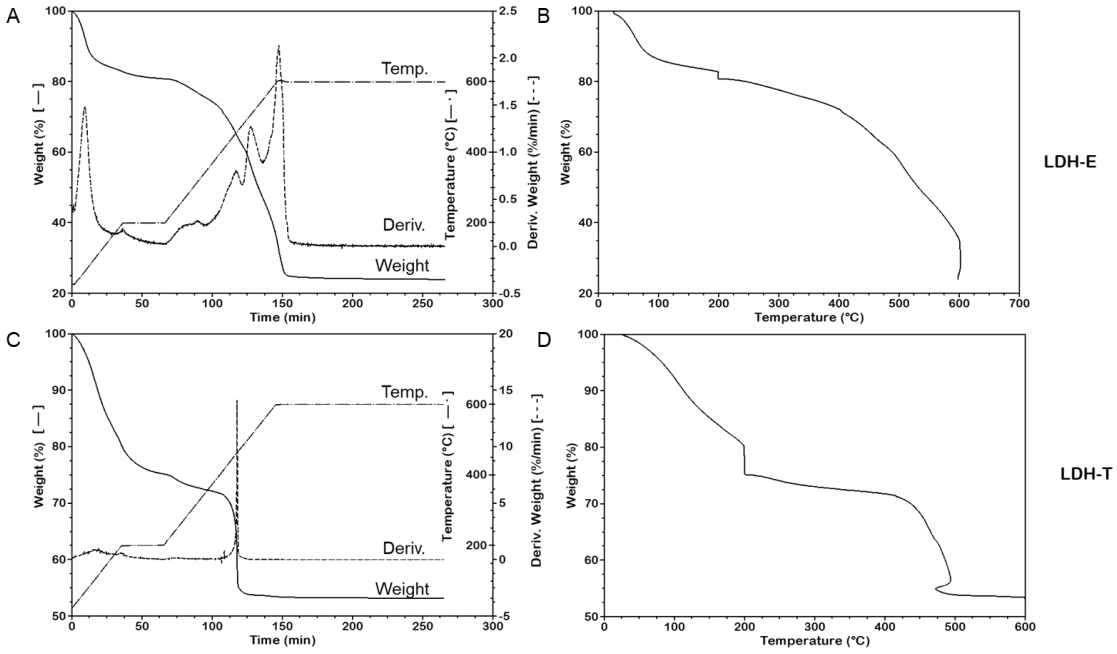

Figure 4. TGA/DTG analysis of LDH-E sample as function of time (A) and temperature (B) and LDH-T sample as function of time (C) and temperature (D).

The optical properties of the synthesized LDH, after drying at 70°C, were evaluated by reflectance spectroscopy. For comparison, pure Eosin Y was also analyzed. Terephthalate containing LDH without Eosin sensibilization (LDH-T) showed no absorbance, i.e. total reflectance, in the visible range, while the presence of Eosin Y intercalated into the LDH structure (LDH-E) provided high absorption in the UV range. Pure Eosin Y powder also presented both high absorption below 300 nm and good absorption in the visible range. When sensitized with Eosin Y, LDH-T was characterized by the absorption peak of Eosin Y at around 530 nm, linked with absorption in UV range (L. Pinto et al., 2019). However, the highest absorbance was displayed by LDH-E, which showed a total absorbance in the range of 200-550 nm that slightly decreased above 550 nm. This indicates that the absorption properties of Eosin Y are maintained even when the molecule is inserted inside the LDH structure, making its application as a photoanode possible. Its higher absorbance compared to the

sensitized LDH is probably related to the higher amount of Eosin Y that can be loaded on the sample by exploiting the LDH interlayer.

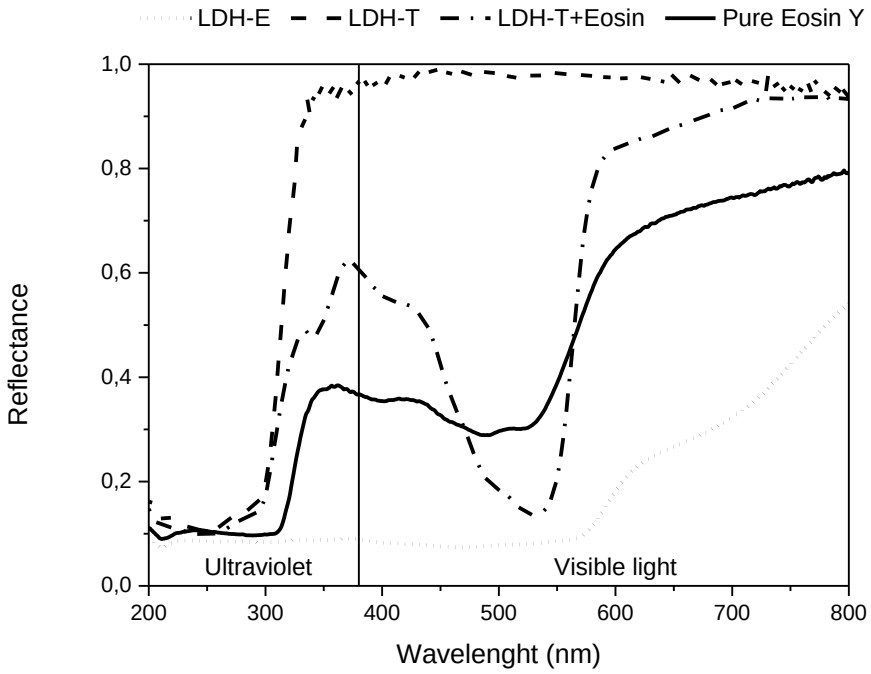

Figure 5. Reflectance spectra of pure Eosin Y, LDH-E, LDH-T and LDH-T+Eosin Y.

3.2 DSSCs tests

Pictures of the LDH-E based ink, the correspondent screen-printed photoanodes and the ones produced with the LDH-T sensitized with ink are reported in Figure 6.

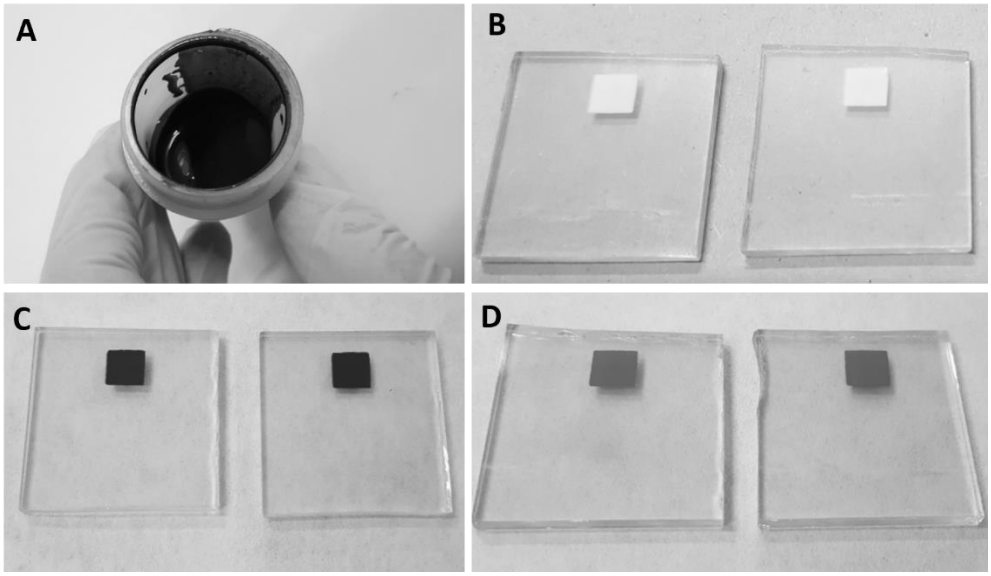

Figure 6. LDH-E screen-printing ink (A) and the related photoanodes(C), the ones based on LDH-T (B) and the LDH-T+Eosin (D).

The Current-Voltage curves in the dark and under illumination are reported in Figure 7 A and B and the extrapolated photovoltaic parameters are reported in Table 2.

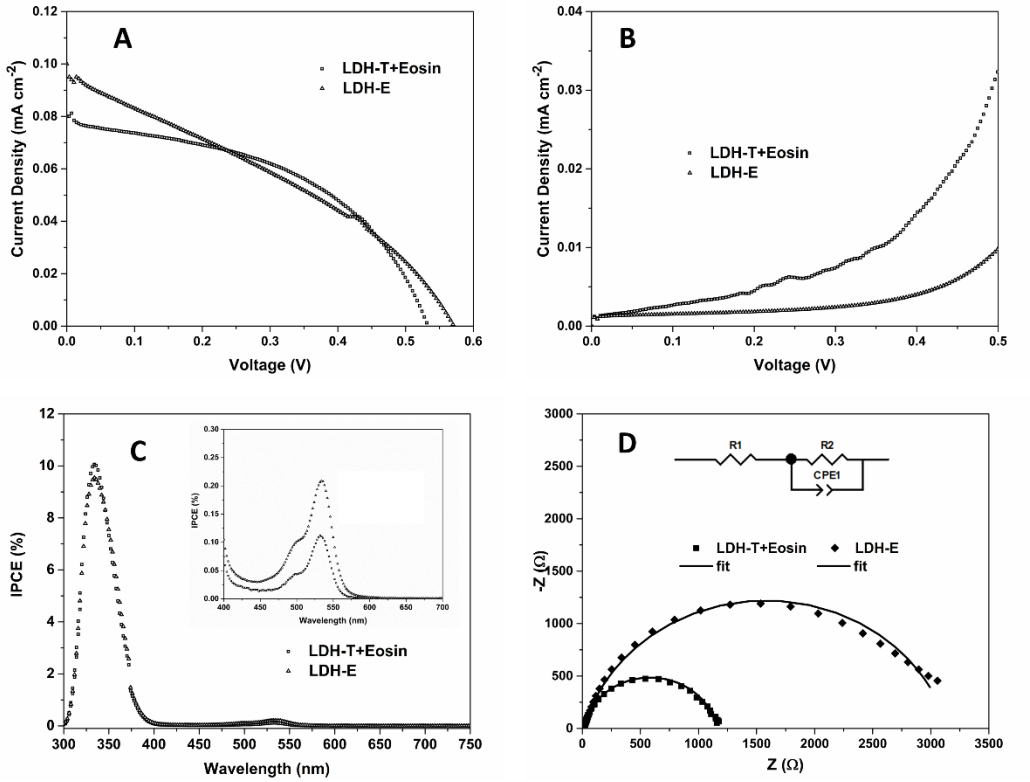

Figure 7. Current-Voltage curves under illumination (A); in the dark (B); IPCE spectra with magnification in the region of Eosin Y absorption (C); Nyquist plots acquired in the dark and equivalent circuit used to fit the experimental points (D).

Table 2. Photovoltaics parameters, efficiencies (PCEs) and IPCE of the prepared DSSCs.

sample	Jsc (mA cm^{-2})	Voc (mV)	FF (%)	PCE (%)	IPCE [a] (%)
LDH-T+Eosin	0.08	532	46	0.019	0.11
LDH-E	0.11	568	30	0.019	0.21

[a] calculated at 534 nm.

The results reported in Table 2 show that the highest current density value (J_{Sc}) was obtained for LDH-E based DSSCs probably due to high light-harvesting produced by the intercalated Eosin Y inside the LDH structure. The IPCE spectra (reported in Figure 7-C and values in Table 2) confirm the trend observed for J_{Sc} with the highest IPCE value (0.21 %) obtained for the DSSC based on the LDH-E photoanode. However, the low Fill Factor (FF) value affects negatively the final PCEs of the LDH-E based devices (as highlighted in the J-V curve reported in Figure 7-A). The whole FF values are limited probably due to the low film adhesion on the FTO substrate and the high internal electrical resistance. In fact, the XRD analyses reported in Figure 3 and Table 1 report a low degree of crystallinity for LDH-E material if compared with LDH-T. Moreover, the highest value of Open Circuit Potential (V_{OC}) of 658 mV was achieved for LDH-E photoanode and this behavior is ascribed to the low recombination rate between the photoanode and the electrolyte. In fact, the onset of the dark current curve (Figure 7 B) occurs at lower bias for LDH-T+Eosin based DSSCs while the ones based on LDH-E suppressed the dark current shifting their onset at higher potentials (Bendoni et al., 2015). Moreover, at the same potential, the lowest quantity of dark current was produced by the LDH-E photoanode. The dye intercalation inside the ZnAl LDH structure therefore reduces the recombination phenomena increasing the V_{OC} value. To explain these results in more detail, EIS analyses in the dark were done on the same devices and the Nyquist plots and equivalent circuit used to fit the experimental points are reported in Figure 7-D. The Nyquist plots show for each DSSC a single semicircle at high and medium frequency due to the high impedance of the devices tested. The main components are related to the photoanode and the photoanode/electrolyte interfaces. In fact, in the equivalent circuit reported in Figure 7-D, R1 describes the electrical resistance of substrate and film while R2 and CPE1 describe the charge-transfer resistance and charge accumulation at the photoanode/electrolyte interface. Considering the R2 values, 1148 Ω, and 3139 Ω were obtained for LDH-T+Eosin and LDH-E respectively, suggesting for the latter a slower charge recombination (Dessì et al., 2015; Mátravölgyi et al., 2017). These results confirm the ones related to the dark current density and explain the highest V_{OC} value obtained for LDH-E photoanode due to the beneficial effect of the Eosin Y intercalation. Finally, the stability of LDH-based DSSCs was evaluated and the results about the main photovoltaics parameters are shown in Figure 8.

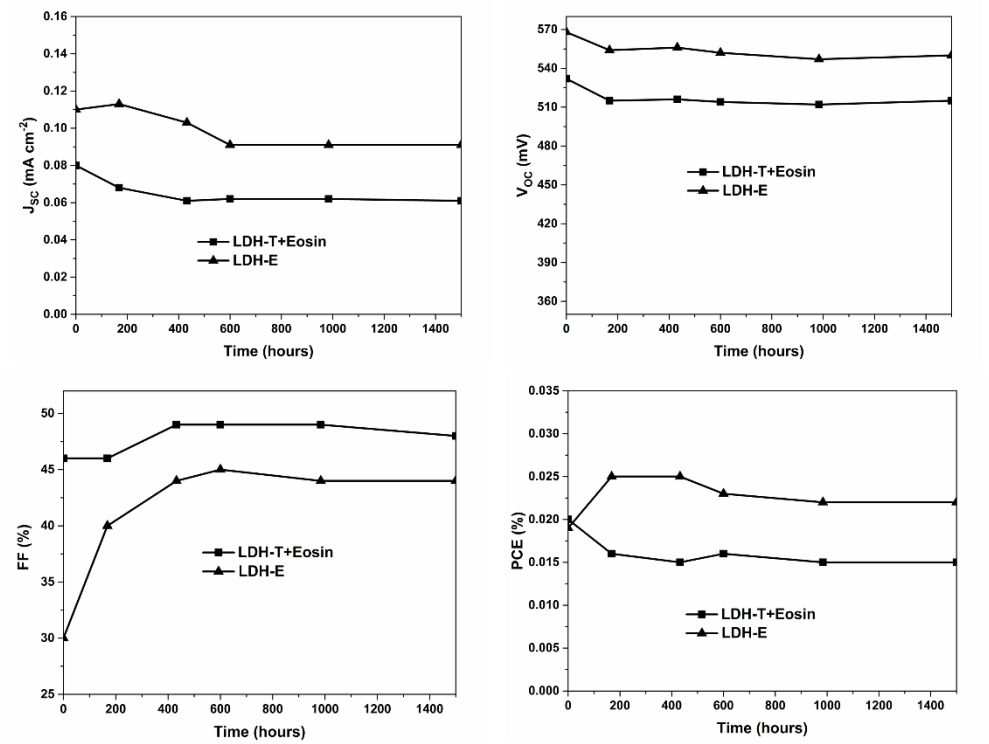

Figure 8. Photovoltaic parameters extrapolated during long-term stability tests (1500 hours).

The results reported in Figure 8 show a higher PCE stability for the DSSCs based on LDH-E than the one based on LDH-T+Eosin. Considering the FF, the device based on LDH-E shows an increase of this parameter during the storage time that finally increases the overall PCE during this time. The same behavior was obtained for J_{SC} that slightly increases for LDH-E devices during the first 200 hours, while it decreases for the LDH-T+Eosin system. These results indicate that an equilibrium occurs between Eosin Y-based photoanodes and the electrolyte after the production of the devices that finally improves their properties. Finally, only the LDH-E photoanode was able to maintain a very stable V_{OC} value up to 1500 hours due to the low amount of recombination inside the cell. The simplified schemes of the working mechanism of the DSSCs based on LDH-T+Eosin and LDH-E are reported in Figure 9.

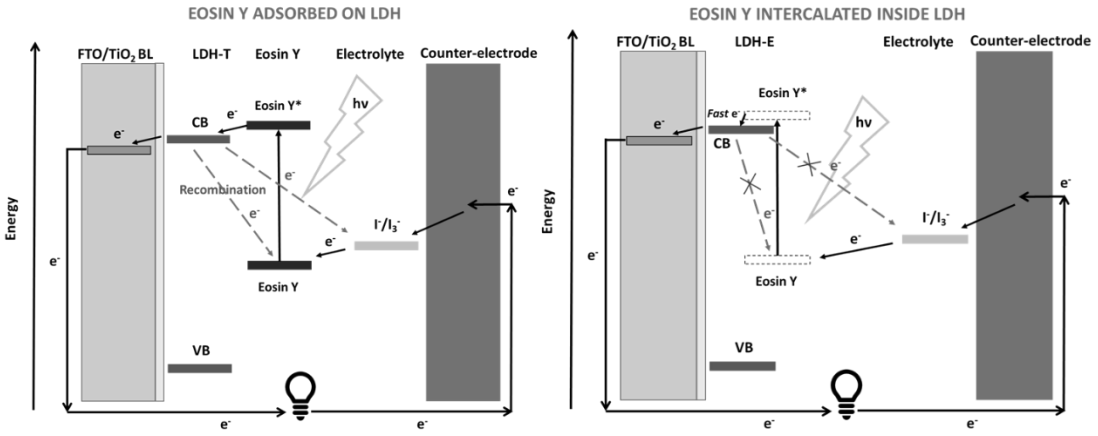

345

346 *Figure 9. Schematic representation of the working mechanism for DSSCs based on (A) sensitized*
347 *LDH with Eosin Y (LDH-T+Eosin) and (B) Eosin Y intercalated into LDH (LDH-E).*

348 When Eosin Y is adsorbed on LDH (LDH-T+Eosin, Figure 9A) photons are absorbed by Eosin Y
349 upon illumination and the photo-generated electrons are injected from the excited state of the dye to
350 the LDH conduction band (CB) and flow thorough the external circuit to the counter-electrode. The
351 dye returns to its ground state by electron transfer from the electrolyte (iodide/triiodide redox system)
352 and finally, an electron transfer occurs from the counter-electrode to the electrolyte to close the
353 circuit. However, EIS analyses and dark current curves show high recombination rate between the
354 photo-generated electrons into CB and the ground state of the dye and electrolyte. When LDH-E
355 photoanode is used, (Figure 9B) the intercalation of Eosin Y molecule inside the LDH structure
356 reduces these recombinations and improve the injection rate of the photo-generated electrons, thus
357 leading the highest Voc and current density and to a more stable device. Based on the improved
358 photo-electron injection from the dye to the LDH sheets, we assume that LDH-E can be represented
359 as a hybrid material able to adsorb light (as reported in Figure 5 with Reflectance spectra) and fastly
360 moving charges.

361 **4. Conclusion**

362 LDH-E was synthesized by a facile one-pot method based on coprecipitation and applied as
363 photoanode in DSSCs. For comparison, an analogous terephthalate intercalated ZnAl LDH was also
364 produced and sensitized with Eosin Y, following a more classical approach for photoanode
365 preparation. Characterization of LDH confirmed the insertion of Eosin Y in the interlayer of its
366 structure, as also shown by TEM analysis. TGA indicated that the interlayered structure was stable
367 up to over 200°C. Eosin Y intercalation into the ZnAl LDH structure increased the stability and
368 efficiency of the DSSCs based on this material. The best performances were obtained for the
369 devices based on LDH-E photoanode due to the key role of Eosin Y inside LDH that decreases the
370 amount of charge recombination phenomena thus increasing the V_{OC} of the correspondent DSSC.

For the same reasons, the stability of the DSSCs based on LDH-E photoanode is increased. These results open the possibility to apply this class of materials in the energy production field, in particular as photoanode for DSSCs. However, the PCE should be improved working on both the increase of the LDH crystallinity and the film adhesion onto the substrates.

Declaration of interests

The authors declare that they have no known competing financial interests or personal relationships that could have appeared to influence the work reported in this paper.

5. References

Abdellaoui, K., Pavlovic, I., Bouhent, M., Benhamou, A., Barriga, C., 2017. A comparative study of the amaranth azo dye adsorption/desorption from aqueous solutions by layered double hydroxides. Applied Clay Science 143, 142–150. https://doi.org/10.1016/j.clay.2017.03.019

Ahmed, A.A.A., Talib, Z.A., Hussein, M.Z. bin, 2012. Thermal, optical and dielectric properties of Zn–Al layered double hydroxide. Applied Clay Science 56, 68–76. https://doi.org/10.1016/j.clay.2011.11.024

Albertazzi, S., Basile, F., Benito, P., Del Gallo, P., Fornasari, G., Gary, D., Rosetti, V., Vaccari, A., 2007. Effect of silicates on the structure of Ni-containing catalysts obtained from hydrotalcite-type precursors. Catalysis Today 128, 258–263.

Arif, M., Yasin, G., Luo, L., Ye, W., Mushtaq, M.A., Fang, X., Xiang, X., Ji, S., Yan, D., 2020. Hierarchical hollow nanotubes of NiFeV-layered double hydroxides@CoVP heterostructures towards efficient, pH-universal electrocatalytical nitrogen reduction reaction to ammonia. Applied Catalysis B: Environmental 265, 118559. https://doi.org/10.1016/j.apcatb.2019.118559

Asif, M., Aziz, A., Azeem, M., Wang, Z., Ashraf, G., Xiao, F., Chen, X., Liu, H., 2018. A review on electrochemical biosensing platform based on layered double hydroxides for small molecule biomarkers determination. Advances in Colloid and Interface Science 262, 21–38. https://doi.org/10.1016/j.cis.2018.11.001

Baig, N., Sajid, M., 2017. Applications of layered double hydroxides based electrochemical sensors for determination of environmental pollutants: A review. Trends in Environmental Analytical Chemistry 16, 1–15. https://doi.org/10.1016/j.teac.2017.10.003

Barkhordari, S., Yadollahi, M., 2016. Carboxymethyl cellulose capsulated layered double hydroxides/drug nanohybrids for Cephalexin oral delivery. Applied Clay Science 121–122, 77–85. https://doi.org/10.1016/j.clay.2015.12.026

Basile, Francesco, Benito, P., Bugani, S., Nolf, W.D., Fornasari, G., Janssens, K., Morselli, L., Scavetta, E., Tonelli, D., Vaccari, A., 2010. Combined Use of Synchrotron-Radiation-Based Imaging Techniques for the Characterization of Structured Catalysts. Advanced Functional Materials 20, 4117–4126. https://doi.org/10.1002/adfm.201001004

Basile, F., Benito, P., Fornasari, G., Gazzoli, D., Pettiti, I., Rosetti, V., Vaccari, A., 2009. Ni-catalysts obtained from silicate intercalated HTlcs active in the catalytic partial oxidation of methane: Influence of the silicate content. Catalysis Today 142, 78–84.

Basile, F, Benito, P., Fornasari, G., Monti, M., Scavetta, E., Tonelli, D., Vaccari, A., 2010. Novel Rh-based structured catalysts for the catalytic partial oxidation of methane. Catalysis Today 157, 183–190.

Basile, F., Fornasari, G., Gazzano, M., Vaccari, A., 2002. Rh, Ru and Ir catalysts obtained by HT precursors: effect of the thermal evolution and composition on the material structure and use. Journal of Materials Chemistry 12, 3296–3303.

Basile, F., Fornasari, G., Livi, M., Tinti, F., Trifirò, F., Vaccari, A., 2004. Performance of new Pt and Pt–Cu on hydrotalcite-derived materials for NOxstorage/reduction. Topics in Catalysis 30, 223–227. https://doi.org/10.1023/B:TOCA.0000029753.61106.ef

Bastianini, M., Vivani, R., Nocchetti, M., Costenaro, D., Bisio, C., Oswald, F., Meyer, T.B., Marchese, L., 2014. Effect of iodine intercalation in nanosized layered double hydroxides for the preparation of quasi-solid electrolyte in DSSC devices. Solar Energy 107, 692–699. https://doi.org/10.1016/j.solener.2014.06.014

Bendoni, R., Barthélémy, A.-L., Sangiorgi, N., Sangiorgi, A., Sanson, A., 2016. Dye-sensitized solar cells based on N719 and cobalt gel electrolyte obtained through a room temperature process. Journal of Photochemistry and Photobiology A: Chemistry 330, 8–14. https://doi.org/10.1016/j.jphotochem.2016.07.021

Bendoni, R., Sangiorgi, N., Sangiorgi, A., Sanson, A., 2015. Role of water in TiO2 screen-printing inks for dye-sensitized solar cells. Solar Energy 122, 497–507. https://doi.org/10.1016/j.solener.2015.09.025

Benesperi, I., Michaels, H., Freitag, M., 2018. The researcher's guide to solid-state dye-sensitized solar cells. Journal of Materials Chemistry C 6, 11903–11942. https://doi.org/10.1039/C8TC03542C

Cao, Y., Li, G., Li, X., 2016. Graphene/layered double hydroxide nanocomposite: Properties, synthesis, and applications. Chemical Engineering Journal 292, 207–223. https://doi.org/10.1016/j.cej.2016.01.114

Cavani, F., Trifiro, F., Vaccari, A., 1991a. Hydrotalcite-type anionic clays: Preparation, properties and applications. Catalysis today 11, 173–301.

Cavani, F., Trifiro, F., Vaccari, A., 1991b. Hydrotalcite-type anionic clays: Preparation, properties and applications. Catalysis today 11, 173–301.

Conterosito, E., Gianotti, V., Palin, L., Boccaleri, E., Viterbo, D., Milanesio, M., 2018. Facile preparation methods of hydrotalcite layered materials and their structural characterization by combined techniques. Inorganica Chimica Acta, Special Volume: Protagonists in Chemistry Dedicated to Professor Carlo Mealli 470, 36–50. https://doi.org/10.1016/j.ica.2017.08.007

Conterosito, E., Van Beek, W., Palin, L., Croce, G., Perioli, L., Viterbo, D., Gatti, G., Milanesio, M., 2013. Development of a Fast and Clean Intercalation Method for Organic Molecules into Layered Double Hydroxides. Crystal Growth & Design 13, 1162–1169. https://doi.org/10.1021/cg301505e

Costantino, U., Ambrogi, V., Nocchetti, M., Perioli, L., 2008. Hydrotalcite-like compounds: versatile layered hosts of molecular anions with biological activity. Microporous and Mesoporous Materials 107, 149–160.

Darie, M., Seftel, E.M., Mertens, M., Ciocarlan, R.G., Cool, P., Carja, G., 2019. Harvesting solar light on a tandem of Pt or Pt-Ag nanoparticles on layered double hydroxides photocatalysts for p-nitrophenol degradation in water. Applied Clay Science 182, 105250. https://doi.org/10.1016/j.clay.2019.105250

Daud, M., Hai, A., Banat, F., Wazir, M.B., Habib, M., Bharath, G., Al-Harthi, M.A., 2019. A review on the recent advances, challenges and future aspect of layered double hydroxides (LDH) – Containing hybrids as promising adsorbents for dyes removal. Journal of Molecular Liquids 288, 110989. https://doi.org/10.1016/j.molliq.2019.110989

Daud, M., Kamal, M.S., Shehzad, F., Al-Harthi, M.A., 2016. Graphene/layered double hydroxides nanocomposites: A review of recent progress in synthesis and applications. Carbon 104, 241–252. https://doi.org/10.1016/j.carbon.2016.03.057

Desigaux, L., Belkacem, M.B., Richard, P., Cellier, J., Léone, P., Cario, L., Leroux, F., Taviot-Guého, C., Pitard, B., 2006. Self-Assembly and Characterization of Layered Double Hydroxide/DNA Hybrids. Nano Lett. 6, 199–204. https://doi.org/10.1021/nl052020a

Dessì, A., Calamante, M., Mordini, A., Peruzzini, M., Sinicropi, A., Basosi, R., Biani, F.F. de, Taddei, M., Colonna, D., Carlo, A. di, Reginato, G., Zani, L., 2015. Thiazolo[5,4- d]thiazole-based organic

sensitizers with strong visible light absorption for transparent, efficient and stable dye-sensitized solar cells. RSC Advances 5, 32657–32668. https://doi.org/10.1039/C5RA03530A

Du, T., Zhu, J., Wang, N., Chen, H., He, H., 2015. Enhanced Photovoltaic Performance of Quasi-Solid Dye-Sensitized Solar Cells Based on Composite Gel Electrolyte with Intercalated Mg-Al Layered Double Hydroxide. J. Electrochem. Soc. 162, H518. https://doi.org/10.1149/2.0461508jes

Fasolini, A., Abate, S., Barbera, D., Centi, G., Basile, F., 2019. Pure H2 production by methane oxy-reforming over Rh-Mg-Al hydrotalcite-derived catalysts coupled with a Pd membrane. Applied Catalysis A: General 581, 91–102. https://doi.org/10.1016/j.apcata.2019.05.024

Foruzin, L.J., Rezvani, Z., Nejati, K., 2019. TiO2@NiAl-Layered double oxide nanocomposite: An excellent photoanode for a dye sensitized solar cell. Solar Energy 186, 106–112. https://doi.org/10.1016/j.solener.2019.05.005

Gao, R., Mei, X., Yan, D., Liang, R., Wei, M., 2018. Nano-photosensitizer based on layered double hydroxide and isophthalic acid for singlet oxygenation and photodynamic therapy. Nature Communications 9, 2798. https://doi.org/10.1038/s41467-018-05223-3

Gao, R., Yan, D., 2017a. Ordered assembly of hybrid room-temperature phosphorescence thin films showing polarized emission and the sensing of VOCs. Chemical Communications 53, 5408–5411. https://doi.org/10.1039/C7CC01794D

Gao, R., Yan, D., 2017b. Layered host–guest long-afterglow ultrathin nanosheets: high-efficiency phosphorescence energy transfer at 2D confined interface. Chemical Science 8, 590–599. https://doi.org/10.1039/C6SC03515A

Gao, R., Yan, D., Evans, D.G., Duan, X., 2017. Layer-by-layer assembly of long-afterglow self-supporting thin films with dual-stimuli-responsive phosphorescence and antiforgery applications. Nano Res. 10, 3606–3617. https://doi.org/10.1007/s12274-017-1571-x

Gjyli, S., Korpa, A., Tabanelli, T., Trettin, R., Cavani, F., Belviso, C., 2019. Higher conversion rate of phenol alkylation with diethylcarbonate by using synthetic fly ash-based zeolites. Microporous and Mesoporous Materials 284, 434–442. https://doi.org/10.1016/j.micromeso.2019.04.065

Guo, Y., Zhu, Z., Qiu, Y., Zhao, J., 2013. Enhanced adsorption of acid brown 14 dye on calcined Mg/Fe layered double hydroxide with memory effect. Chemical engineering journal 219, 69–77.

Iftekhar, S., Srivastava, V., Sillanpää, M., 2017. Synthesis and application of LDH intercalated cellulose nanocomposite for separation of rare earth elements (REEs). Chemical Engineering Journal 309, 130–139. https://doi.org/10.1016/j.cej.2016.10.028

Iyi, N., Yamada, H., Sasaki, T., 2011. Deintercalation of carbonate ions from carbonate-type layered double hydroxides (LDHs) using acid–alcohol mixed solutions. Applied Clay Science 54, 132–137. https://doi.org/10.1016/j.clay.2011.07.017

Jin, L., Zeng, H.-Y., Du, J.-Z., Xu, S., 2020. Intercalation of organic and inorganic anions into layered double hydroxides for polymer flame retardancy. Applied Clay Science 187, 105481. https://doi.org/10.1016/j.clay.2020.105481

J. Wu, M., Z. Wu, J., Zhang, J., Chen, H., Z. Zhou, J., R. Qian, G., P. Xu, Z., Du, Z., L. Rao, Q., 2018. A review on fabricating heterostructures from layered double hydroxides for enhanced photocatalytic activities. Catalysis Science & Technology 8, 1207–1228. https://doi.org/10.1039/C7CY02314F

Káfuňková, E., Lang, K., Kubát, P., Klementová, M., Mosinger, J., Šlouf, M., Troutier-Thuilliez, A.-L., Leroux, F., Verney, V., Taviot-Guého, C., 2010. Porphyrin -layered double hydroxide / polymer composites as novel ecological photoactive surfaces. Journal of Materials Chemistry 20, 9423–9432. https://doi.org/10.1039/C0JM00746C

Kang, H., Huang, G., Ma, S., Bai, Y., Ma, H., Li, Y., Yang, X., 2009. Coassembly of Inorganic Macromolecule of Exfoliated LDH Nanosheets with Cellulose. J. Phys. Chem. C 113, 9157–9163. https://doi.org/10.1021/jp900861k

Ladewig, K., Xu, Z.P., Lu, G.Q. (Max), 2009. Layered double hydroxide nanoparticles in gene and drug delivery. Expert Opinion on Drug Delivery 6, 907–922. https://doi.org/10.1517/17425240903130585

514 Li, Y., Tang, L., Ma, X., Wang, X., Zhou, W., Bai, D., 2017. Synthesis and characterization of Zn-Ti layered
515 double hydroxide intercalated with cinnamic acid for cosmetic application. Journal of Physics and
516 Chemistry of Solids 107, 62–67. https://doi.org/10.1016/j.jpcs.2017.02.018
517 Liu, S., Liu, Jianqiang, Wang, T., Wang, C., Ge, Z., Liu, Jie, Hao, X., Du, N., Xiao, H., 2019. Preparation and
518 photovoltaic properties of dye-sensitized solar cells based on zinc titanium mixed metal oxides.
519 Colloids and Surfaces A: Physicochemical and Engineering Aspects 568, 59–65.
520 https://doi.org/10.1016/j.colsurfa.2019.02.005
521 L. Pinto, A., Jorge Parola, A., P. Leal, J., B. Coutinho, I., L. Pereira, C.C., 2019. Dye-sensitized solar cells using
522 fluorone-based ionic liquids with improved cell efficiency. Sustainable Energy & Fuels 3, 3510–
523 3517. https://doi.org/10.1039/C9SE00783K
524 Luo, L., Wang, Z., Xiang, X., Yan, D., Ye, J., 2020. Selective Activation of Benzyl Alcohol Coupled with
525 Photoelectrochemical Water Oxidation via a Radical Relay Strategy. ACS Catal. 10, 4906–4913.
526 https://doi.org/10.1021/acscatal.0c00660
527 Mátravölgyi, B., Hergert, T., Thurner, A., Varga, B., Sangiorgi, N., Bendoni, R., Zani, L., Reginato, G.,
528 Calamante, M., Sinicropi, A., Sanson, A., Faigl, F., Mordini, A., 2017. Synthesis and Investigation of
529 Solar-Cell Photosensitizers Having a Fluorazone Backbone. European Journal of Organic Chemistry
530 2017, 1843–1854. https://doi.org/10.1002/ejoc.201601622
531 Meng, W., Li, F., Evans, D.G., Duan, X., 2004. Preparation and intercalation chemistry of magnesium–
532 iron(III) layered double hydroxides containing exchangeable interlayer chloride and nitrate ions.
533 Materials Research Bulletin 39, 1185–1193. https://doi.org/10.1016/j.materresbull.2004.04.016
534 Milanesio, M., Conterosito, E., Viterbo, D., Perioli, L., Croce, G., 2010. New efficient intercalation of
535 bioactive molecules into layered double hydroxide materials by solid-state exchange: an in situ
536 XRPD study. Crystal growth & design 10, 4710–4712.
537 Mishra, G., Dash, B., Pandey, S., 2018. Layered double hydroxides: A brief review from fundamentals to
538 application as evolving biomaterials. Applied Clay Science 153, 172–186.
539 https://doi.org/10.1016/j.clay.2017.12.021
540 Mohapatra, L., Parida, K., 2016. A review on the recent progress, challenges and perspective of layered
541 double hydroxides as promising photocatalysts. Journal of Materials Chemistry A 4, 10744–10766.
542 https://doi.org/10.1039/C6TA01668E
543 Monti, M., Benito, P., Basile, F., Fornasari, G., Gazzano, M., Scavetta, E., Tonelli, D., Vaccari, A., 2013.
544 Electrosynthesis of Ni/Al and Mg/Al Layered Double Hydroxides on Pt and FeCrAlloy supports:
545 Study and control of the pH near the electrode surface. Electrochimica Acta 108, 596–604.
546 https://doi.org/10.1016/j.electacta.2013.06.143
547 Oh, J.-M., Kwak, S.-Y., Choy, J.-H., 2006. Intracrystalline structure of DNA molecules stabilized in the layered
548 double hydroxide. Journal of Physics and Chemistry of Solids, Proceedings of the 13th International
549 Symposium on Intercalation Compounds, Clermont-Frerrand, France, 6-9 June, 2005 67, 1028–
550 1031. https://doi.org/10.1016/j.jpcs.2006.01.080
551 Park, N.-G., 2015. Perovskite solar cells: an emerging photovoltaic technology. Materials Today 18, 65–72.
552 https://doi.org/10.1016/j.mattod.2014.07.007
553 Prasad, C., Tang, H., Liu, Q.Q., Zulfiqar, S., Shah, S., Bahadur, I., 2019. An overview of
554 semiconductors/layered double hydroxides composites: Properties, synthesis, photocatalytic and
555 photoelectrochemical applications. Journal of Molecular Liquids 289, 111114.
556 https://doi.org/10.1016/j.molliq.2019.111114
557 Rasouli, N., 2018. Application of a novel, efficient and recyclable photo redox catalyst (Zn–Al layered double
558 hydroxide/eosin) for the synthesis of substituted pyridine derivatives under visible light irradiation.
559 Applied Organometallic Chemistry 32, e4585. https://doi.org/10.1002/aoc.4585
560 Rives, V., Angeles Ulibarri, M., 1999. Layered double hydroxides (LDH) intercalated with metal coordination
561 compounds and oxometalates. Coordination Chemistry Reviews 181, 61–120.
562 https://doi.org/10.1016/S0010-8545(98)00216-1
563 Salih, E.Y., Sabri, M.F.M., Tan, S.T., Sulaiman, K., Hussein, M.Z., Said, S.M., Yap, C.C., 2019. Preparation and
564 characterization of ZnO/ZnAl2O4-mixed metal oxides for dye-sensitized photodetector using Zn/Al-

layered double hydroxide as precursor. J Nanopart Res 21, 55. https://doi.org/10.1007/s11051-019-4501-x
Sangiorgi, A., Bendoni, R., Sangiorgi, N., Sanson, A., Ballarin, B., 2014. Optimized TiO2 blocking layer for dye-sensitized solar cells. Ceramics International 40, 10727–10735. https://doi.org/10.1016/j.ceramint.2014.03.060
Shahabadi, N., Razlansari, M., 2018. Biological Application of Layered Double Hydroxides in Drug Delivery Systems. Journal of Nanoanalysis 5, 210–226. https://doi.org/10.22034/jna.2018.545418
Tabanelli, T., Passeri, S., Guidetti, S., Cavani, F., Lucarelli, C., Cargnoni, F., Mella, M., 2019. A cascade mechanism for a simple reaction: The gas-phase methylation of phenol with methanol. Journal of Catalysis 370, 447–460. https://doi.org/10.1016/j.jcat.2019.01.014
Tadanaga, K., Oi, J., Higuchi, M., 2016. Preparation of Zn–Al layered double hydroxide thin films intercalated with Eosin Y by hot water treatment of sol-gel derived precursor films. Journal of Sol-Gel Science and Technology 79, 303–307.
Tang, S., Yao, Y., Chen, T., Kong, D., Shen, W., Lee, H.K., 2020. Recent advances in the application of layered double hydroxides in analytical chemistry: A review. Analytica Chimica Acta 1103, 32–48. https://doi.org/10.1016/j.aca.2019.12.065
Vucelic, M., Moggridge, G., Jones, W., 1995. Thermal properties of terephthalate-and benzoate-intercalated LDH. The Journal of Physical Chemistry 99, 8328–8337.
Wang, Y., Yan, D., Hankari, S.E., Zou, Y., Wang, S., 2018. Recent Progress on Layered Double Hydroxides and Their Derivatives for Electrocatalytic Water Splitting. Advanced Science 5, 1800064. https://doi.org/10.1002/advs.201800064
Wypych, F., Bubniak, G.A., Halma, M., Nakagaki, S., 2003. Exfoliation and immobilization of anionic iron porphyrin in layered double hydroxides. Journal of Colloid and Interface Science 264, 203–207. https://doi.org/10.1016/S0021-9797(03)00374-6
Xu, Z.P., Zhang, J., Adebajo, M.O., Zhang, H., Zhou, C., 2011. Catalytic applications of layered double hydroxides and derivatives. Applied Clay Science, Clay Mineral-based Catalysts and Catalysis 53, 139–150. https://doi.org/10.1016/j.clay.2011.02.007
Yadollahi, M., Namazi, H., Barkhordari, S., 2014. Preparation and properties of carboxymethyl cellulose/layered double hydroxide bionanocomposite films. Carbohydrate Polymers 108, 83–90. https://doi.org/10.1016/j.carbpol.2014.03.024
Yang, F., Sun, S., Chen, X., Chang, Y., Zha, F., Lei, Z., 2016. Mg–Al layered double hydroxides modified clay adsorbents for efficient removal of Pb2+, Cu2+ and Ni2+ from water. Applied Clay Science 123, 134–140. https://doi.org/10.1016/j.clay.2016.01.026
Yang, Z., Wang, F., Zhang, C., Zeng, G., Tan, X., Yu, Z., Zhong, Y., Wang, H., Cui, F., 2016. Utilization of LDH-based materials as potential adsorbents and photocatalysts for the decontamination of dyes wastewater: a review. RSC Advances 6, 79415–79436. https://doi.org/10.1039/C6RA12727D
Zaghouane-Boudiaf, H., Boutahala, M., Arab, L., 2012. Removal of methyl orange from aqueous solution by uncalcined and calcined MgNiAl layered double hydroxides (LDHs). Chemical Engineering Journal 187, 142–149. https://doi.org/10.1016/j.cej.2012.01.112
Zhang, G., Zhang, X., Meng, Y., Pan, G., Ni, Z., Xia, S., 2020. Layered double hydroxides-based photocatalysts and visible-light driven photodegradation of organic pollutants: A review. Chemical Engineering Journal 392, 123684. https://doi.org/10.1016/j.cej.2019.123684
Zhang, T., Shang, H., Zhang, B., Yan, D., Xiang, X., 2021. Ag/Ultrathin-Layered Double Hydroxide Nanosheets Induced by a Self-Redox Strategy for Highly Selective CO2 Reduction. ACS Appl. Mater. Interfaces 13, 16536–16544. https://doi.org/10.1021/acsami.1c02737
Zhu, Y., Wang, D., Yang, X., Liu, S., Liu, D., Liu, Jie, Xiao, H., Hao, X., Liu, Jianqiang, 2017. Investigation of the dye-sensitized solar cell designed by a series of mixed metal oxides based on ZnAl-layered double hydroxide. Appl. Phys. A 123, 641. https://doi.org/10.1007/s00339-017-1256-z
Zubair, M., Daud, M., McKay, G., Shehzad, F., Al-Harthi, M.A., 2017. Recent progress in layered double hydroxides (LDH)-containing hybrids as adsorbents for water remediation. Applied Clay Science 143, 279–292. https://doi.org/10.1016/j.clay.2017.04.002

617